



This discussion paper is/has been under review for the journal Atmospheric Measurement Techniques (AMT). Please refer to the corresponding final paper in AMT if available.

Aerosol retrieval from RSP measurements

L. Wu et al.

Aerosol retrieval from multiangle multispectral photopolarimetric measurements: importance of spectral range and angular resolution

L. Wu^{1,4}, O. Hasekamp¹, B. van Dierenhoven^{2,3}, and B. Cairns³

¹SRON Netherlands Institute for Space Research, Sorbonnelaan 2, 3584 CA Utrecht, the Netherlands

²Columbia University, Center for Climate System Research, New York, NY, USA

³NASA Goddard Institute for Space Studies, New York, NY, USA

⁴School of Computer and Information, Hefei University of Technology, Hefei, Anhui 230009, China

Received: 18 February 2015 – Accepted: 2 March 2015 – Published: 13 March 2015

Correspondence to: L. Wu (l.wu@sron.nl)

Published by Copernicus Publications on behalf of the European Geosciences Union.

Title Page

Abstract

Introduction

Conclusions

References

Tables

Figures



Back

Close

Full Screen / Esc

Printer-friendly Version

Interactive Discussion



Abstract

We investigated the importance of spectral range and angular resolution for aerosol retrieval from multi-angle photo-polarimetric measurements over land. For this purpose, we use an extensive set of simulated measurements for different spectral ranges and angular resolutions and subsets of real measurements of the airborne Research Scanning Polarimeter (RSP) carried out during the PODEX and SEAC⁴RS campaigns over continental US. Aerosol retrievals performed from RSP measurements show good agreement with ground based AERONET measurements for AOT, SSA, and refractive index. Furthermore, we found that inclusion of shortwave infrared bands (1590 and/or 2250 nm) significantly improves the retrieval of AOT, SSA and coarse mode microphysical properties. On the other hand, retrieval accuracies on aerosol properties do not improve significantly if more than 10 viewing angles are used in the retrieval.

1 Introduction

The radiative impact caused by aerosols is widely considered to be one of the largest uncertainties in the radiative forcing of the earth climate (IPCC, 2013). Aerosols influence the radiative balance of the Earth by scattering and absorbing solar radiation. A major issue for the evaluation of aerosols in climate models is the limited accuracy and detail of global measurements of the aerosol properties required for climate modelling, such as particle size distribution, shape, complex refractive index and columnar concentration. Orbital remote sensing instruments that perform multi-angle, multi-spectral photopolarimetric measurements have the capability to provide these aerosol properties with the required accuracy (Mishchenko and Travis, 1997; Hasekamp and Landgraf, 2007). The advantages of polarimetric measurements over intensity-only measurements come from the sensitivity of polarization of light and its spectral and angular dependence to particle size, shape and refractive index. The Polarization and Directionality of the Earth's Reflectance (POLDER), the most recent in-orbit polarization-

AMTD

8, 2793–2822, 2015

Aerosol retrieval from RSP measurements

L. Wu et al.

Title Page

Abstract

Introduction

Conclusions

References

Tables

Figures



Back

Close

Full Screen / Esc

Printer-friendly Version

Interactive Discussion



**Aerosol retrieval from
RSP measurements**

L. Wu et al.

[Title Page](#)[Abstract](#)[Introduction](#)[Conclusions](#)[References](#)[Tables](#)[Figures](#)[Back](#)[Close](#)[Full Screen / Esc](#)[Printer-friendly Version](#)[Interactive Discussion](#)

measuring satellite instrument, has demonstrated the importance of polarization measurements for the retrieval of aerosol properties (Hasekamp et al., 2011; Dubovik et al., 2011). Limitations of the POLDER instrument are its inherent limited polarimetric accuracy and its relatively small spectral range. To overcome these limitations, the Aerosol Polarimetry Sensor (APS) was scheduled for launch in Glory mission. This instrument was designed to view a scene from ~ 250 viewing angles in nine spectral bands ranging from 410 to 2250 nm. Due to the tragedy of the Glory launch failure, space-borne multi-angle photo polarimetric measurements are currently unavailable. However, the Research Scanning Polarimeter (RSP) that has similar characteristics as APS continues to perform airborne measurements in many field campaigns. The collected data will facilitate algorithm development and allow us to derive geophysically relevant aerosol and cloud properties (Waquet et al., 2009a).

RSP provides measurements of a ground scene at ~ 152 different viewing angles ($\pm 60^\circ$ from nadir) in nine spectral bands from visible-near-infrared bands to short-wave infrared bands (410, 470, 550, 670, 865, 960, 1590, 1880 and 2250 nm). The measurements provide the first three Stokes parameters, I , Q and U in the nine spectral channels with a radiometric uncertainty of $\sim 2.0\%$ and a polarimetric uncertainty of $\sim 0.2\%$ (Cairns et al., 1999). Given its large spectral range and number of viewing angles, RSP measurements are well suited to study the importance of spectral range and angular resolution for the retrieval of aerosol properties. These are two important design parameters for future polarimetric instrumentation, like 3MI onboard EPS-SG (EUMETSAT Polar System-Second Generation).

In this paper we apply an extended version of the SRON aerosol retrieval algorithm (Hasekamp et al., 2011) to several subsets of RSP measurements over land in order to investigate the importance of spectral range and angular resolution of multi-angle photo-polarimetric instrumentation for aerosol retrieval. In addition, we also study the above mentioned aspects using an extensive set of synthetic measurements. Although studies using synthetic multi-angle photo-polarimetric measurements have been published before (Hasekamp and Landgraf, 2007; Hasekamp, 2010; Knobelspiesse et al.,

2012; Ottaviani et al., 2013), they were all based on linear error propagation and a limited number of aerosol scenarios. Instead, here we perform a full iterative retrieval on the synthetic measurements and consider a large number of aerosol scenarios. Therefore, the synthetic study included in this paper is an extension of the above mentioned synthetic studies.

In order to exploit the full spectral range of RSP, we extend the SRON aerosol retrieval algorithm to be capable to cope with spectrally dependent refractive index. The paper is organized as follows: Sect. 2 describes the data used in the paper, Sect. 3 describes the retrieval method, Sect. 4 shows the results based on synthetic measurements, and Sect. 5 shows the results based on RSP measurements. Finally, Sect. 6 concludes the paper.

2 Data

The used RSP data in the paper are obtained during the PODEX (Polarimeter Definition Experiment) campaign and SEAC⁴RS (Studies of Emissions and Atmospheric Composition, Clouds and Climate Coupling by Regional Surveys) campaign in 2013. While the objectives for both campaigns include studies for future instrument design, SEAC⁴RS also seeks to improve our understanding of feedbacks of aerosols on meteorology and climate (Toon, 2013). The PODEX and SEAC⁴RS measurements were acquired over continental US with RSP instrument mounted on ER-2 high-altitude aircraft, which flies at an altitude of approximately 20 km with speed around 200 ms⁻¹. During the SEAC⁴RS campaign, a number of AERONET sites co-located with the ER-2 flight track are available; thus we can compare aerosol properties obtained from RSP measurements with corresponding AERONET aerosol products.

For both campaigns, we focus on measurements of the RSP bands at 410, 470, 550, 670, 865, 1590, and 2250 nm. The 960 and 1880 nm bands are excluded, because their main purposes are water vapor estimation and cirrus cloud screening characterization. For each spectral band, we only use viewing angles in the range $[-60, 40^\circ]$ because

Aerosol retrieval from RSP measurements

L. Wu et al.

Title Page

Abstract

Introduction

Conclusions

References

Tables

Figures



Back

Close

Full Screen / Esc

Printer-friendly Version

Interactive Discussion



Aerosol retrieval from RSP measurementsL. Wu et al.

[Title Page](#)[Abstract](#)[Introduction](#)[Conclusions](#)[References](#)[Tables](#)[Figures](#)[◀](#)[▶](#)[◀](#)[▶](#)[Back](#)[Close](#)[Full Screen / Esc](#)[Printer-friendly Version](#)[Interactive Discussion](#)

some of the viewing angles are blocked by the ER-2 aircraft. We use the data that have already been aggregated to ground level. Due to imperfect co-registration of different viewing angles, the angular measurements show oscillations larger than the measurement error for inhomogeneous scenes. In order to reduce this effect we average RSP measurements over a distance of 5 km so that mis-registrations between viewing angles become small compared to the effective pixel size. Figure 1 shows an example of a RSP measurement for an individual ground pixel and for an effective 5 km averaged pixel.

In the retrieval, information on temperature, pressure, and relative humidity profiles in atmosphere is interpolated to a particular date, time and location of the RSP measurements using NCEP reanalysis data (Kistler et al., 2001).

3 Methods

3.1 Forward model

In the PODEX and SEAC⁴RS campaigns, the airborne RSP measurements are performed at altitude around 20 km in the atmosphere. To model the radiance and state of polarization of light at a given wavelength at the RSP flight altitude, we consider a macroscopically isotropic, plane-parallel multi-layered atmosphere bounded below by a reflecting surface. Each atmosphere layer is characterized by scattering and absorption optical thickness and the scattering phase matrix \mathbf{P} .

For RSP shortwave infrared bands, gaseous absorption need to be taken into account. The absorption in RSP 1590 and 2250 nm bands can be represented by a model that is derived using k distributions for each 1 nm that are then integrated with a solar weighting over the RSP bandpasses. Here the total absorption optical depth depends on the total column optical depth of well-mixed gases and water vapor. It should be noted that water vapor absorption is relatively small if compared with that of the well mixed gases CO₂ at 1590 nm and methane at 2250 nm. In terms of profile distribu-

tions, the integrated optical depths from the top of the atmosphere to a pressure level p for the well-mixed gases and water vapor are proportional to $(p/p_0)^2$ and $(p/p_0)^4$ respectively, where p_0 is the surface pressure.

The optical properties of aerosols depend on the size, shape and type of aerosols.

There is sufficient evidence that mixtures of spheroids allow rather accurate fitting of measured spectral and angular dependencies of observed intensity and polarization (Dubovik et al., 2006). Here we consider scattering properties of both spherical and spheroidal aerosol particles. The optical properties of spherical and spheroidal aerosol particles are calculated using the tabulated kernels for spheroids and spheres of Dubovik et al. (2006). Here we describe particles as a mixture of spheres and spheroids with the aspect ratio distribution proposed by Dubovik et al. (2006).

For surface reflection characterization of RSP data, the Rahman Pinty Verstraete model (RPV) (Rahman et al., 1993) is used with three independent parameters ρ_0 , g and k (see Appendix). The model successfully accounts for the observed variability of reflectance measurements in laboratory and field conditions, ranging from bare soil to full canopy cover, in both the visible and the near-infrared bands (Rahman et al., 1993). To account for surface polarized reflectance, we use a modified Fresnel model introduced by Litvinov et al. (2011) (see Appendix). It has been shown that the BRDF and BPDF models used here can fit the RSP measurements with sufficient accuracy (Litvinov et al., 2011).

We solve the vector radiative transfer equation in the Earth atmosphere using the method as described by Hasekamp and Landgraf (2002, 2005a). To solve the integration over azimuth angle, the radiative transfer equations are decomposed into a series of Fourier components. To reduce the number of terms needed in the Fourier series, the single scattering is calculated analytically. To efficiently treat highly peaked phase function we apply the “MS method” by Nakajima and Tanaka (1988). Then, an iterative Gauss–Seidel method is applied to solve the radiative transfer equations (Herman and Browning, 1965; Landgraf et al., 2001; Schepers et al., 2014).

Aerosol retrieval from RSP measurements

L. Wu et al.

Title Page

Abstract

Introduction

Conclusions

References

Tables

Figures



Back

Close

Full Screen / Esc

Printer-friendly Version

Interactive Discussion



3.2 Retrieval method

The aim of aerosol retrieval is to convert observed measurements into information about physical properties of aerosols, i.e.,

$$(\mathbf{y}) = \mathbf{F}((\mathbf{x})) + (\mathbf{e})_y. \quad (1)$$

5 Here (\mathbf{y}) is the measurement vector that contains the multiple-wavelength multiple-viewing angle measurements including radiance and degree of linear polarization (DOLP), \mathbf{F} is the forward radiative transfer model and $(\mathbf{e})_y$ is an error term. To define the state vector (\mathbf{x}) , we employ the bimodal lognormal function to describe the atmospheric aerosol size distributions including a small and coarse mode indicated by superscripts s and c . Here, each mode is characterized by the effective radius r_{eff} , the effective variance v_{eff} and aerosol loading N which is the number of aerosol particles per square meter. Spherical and spheroidal aerosol particles are distinguished by fraction ratio p , which indicate the percentage of spheroid particles in aerosol loading N . We consider a Gaussian height distribution for aerosol layers and include the height parameter as one additional unknown parameter in our retrieval.

15 Additionally, the complex refractive index $m = m_r + im_i$, is needed to characterize aerosols of each mode. Figure 2 shows the spectral dependence of the most important aerosol types (D’Almeida et al., 1991). It can be seen in Fig. 2 that for the aerosol types that pre dominantly occur in the small mode (biomass burning, industrial, soot, sulfate, and water soluble) the spectral dependence of the real refractive index is relatively flat in the spectral range where they are mostly optically active (< 1200 nm). Although the imaginary part for the small mode types shows spectral dependence for some types, the values for these types are already very small so that the wavelength dependence will not significantly affect optical measurements in the visible spectral range. This may be different if Brown Carbon would be included in the analysis (Feng et al., 2013). For the coarse mode, the situation is different, since most real refractive indices show spectral dependence in the range $> \sim 1200$ nm where coarse mode aerosols are optically

Aerosol retrieval from RSP measurements

L. Wu et al.

Title Page

Abstract

Introduction

Conclusions

References

Tables

Figures

◀

▶

◀

▶

Back

Close

Full Screen / Esc

Printer-friendly Version

Interactive Discussion



active. Further, for dust the imaginary part of the refractive index increases strongly in the blue/UV part of the spectrum. In a straightforward way, the spectral variations of refractive index of coarse mode aerosols can be described by a linear combination of the three coarse mode aerosols in Fig. 2. If so, we have six parameters to be fit for both real and imaginary part of refractive index of coarse mode aerosols. However, we find that these six parameters are strongly intercorrelated, so in fact less than six parameters are needed. The well-known principle component analysis (PCA) method can be used to determine the most important spectral signatures in the refractive index (Smith, 2002). For the real part of complex refractive index, a $t \times n$ matrix \mathbf{M} with $n \geq t$ is constructed as,

$$\mathbf{M} = [(\mathbf{m})_1, (\mathbf{m})_2, \dots, (\mathbf{m})_t]^T, \quad (2)$$

where T indicate the transposed vector and row vectors are mean-subtracted real part of the refractive indexes at n different wavelengths for t types of representative coarse mode aerosols. From the covariance matrix of \mathbf{M} , eigenvectors $(\mathbf{m})_i^d$ can be derived in order of significance indicated by eigenvalues. We order the vector $(\mathbf{m})_i^d$ according to their eigenvalues and map them into the original data space by multiplying with \mathbf{M} . Consequently, the original row vectors in matrix \mathbf{M} or their linear combinations can be exactly reconstructed by wavelength dependent vector $(\mathbf{m})_i^d$ and wavelength independent value m^{ind} through

$$(\mathbf{m}) = m^{\text{ind}} + \sum_{i=1}^{t'} \alpha_i \cdot (\mathbf{m})_i^d, \quad (3)$$

with $t' = t$ and α_i is the weight of vector $(\mathbf{m})_i^d$. For coarse mode aerosols in Fig. 2, we found that for $t' = 1$ we can sufficiently describe the spectral features in the refractive index, both for the real and imaginary part.

In total, for coarse mode aerosols there are 8 state vector elements, of which two correspond to size (r_{eff} and v_{eff}), four correspond to refractive index (m_r^{ind} , α_r , m_i^{ind} and α_i),

Aerosol retrieval from RSP measurements

L. Wu et al.

Title Page

Abstract

Introduction

Conclusions

References

Tables

Figures



Back

Close

Full Screen / Esc

Printer-friendly Version

Interactive Discussion



one for aerosol loading N and one for the spheroid fraction ρ . The small mode aerosols are described in the same way with 5 state vector elements, i.e. without the parameters describing spectral dependence of the refractive index and the spheroid fraction. In the retrieval, we also consider to retrieve aerosol height parameter of the Gaussian height distribution. As a consequence, the state vector (\mathbf{x}) contains 14 aerosol related elements in total. In addition to these aerosol parameters we also include the surface reflection parameters ρ_0 , g and k of RPV model and surface polarized reflectance parameters α and σ of the modified Fresnel model in the state vector.

To retrieve the state vector (\mathbf{x}) from RSP measurements, an inversion algorithm based on the Phillips–Tikhonov regularization is employed (Hasekamp and Landgraf, 2005b), which has been successfully applied to aerosol retrieval from PARASOL measurements (Hasekamp et al., 2011). The inversion algorithm chooses the solution ($\hat{\mathbf{x}}$) that solves the minimization problem

$$\hat{\mathbf{x}} = \min_{(\mathbf{x})} \left(\left\| \mathbf{S}_y^{-\frac{1}{2}} (\mathbf{F}(\mathbf{x})) - (\mathbf{y}) \right\|^2 + \gamma \left\| \mathbf{W}((\mathbf{x}) - (\mathbf{x})_a) \right\|^2 \right), \quad (4)$$

where $(\mathbf{x})_a$ is a priori state vector, \mathbf{W} is a weighting matrix, and \mathbf{S}_y is the measurement error covariance matrix which contains the measurement error estimate. The weighting matrix \mathbf{W} is chosen diagonal such that $W_{ij} = 1/x_{a,j}$ making the side constraint dimensionless. The regularization parameter γ can be found from the L curve (Hansen and O’Leary, 1993). For more details, we refer to the paper of Hasekamp et al. (2011).

To obtain an appropriate first guess state vector for the iterative retrieval procedure, we perform a look-up table based retrieval based on 48 aerosol modes for the small mode and 24 for the coarse mode. In the small mode, we have 4 equidistant points for $r_{\text{eff}}^{\text{S}}$ between 0.05 and 0.30, 4 equidistant points for m_r^{S} between 1.37 and 1.60, 1 point of 0.19 for $v_{\text{eff}}^{\text{S}}$, and 3 points of -0.001 , -0.02 and -0.1 for m_i^{S} . In the coarse mode, we have 2 points of 1.00 and 2.50 for $r_{\text{eff}}^{\text{C}}$, 3 equidistant points for m_r^{C} between 1.38 and 1.50, 1 point of 0.43 for $v_{\text{eff}}^{\text{C}}$, 2 points of -0.001 and -0.05 for m_i^{C} , and 2 points of 0.1 and 1.0 for ρ . For aerosol optical thickness (AOT), we use 9 point of AOT for each mode

Aerosol retrieval from RSP measurements

L. Wu et al.

Title Page

Abstract

Introduction

Conclusions

References

Tables

Figures

◀

▶

◀

▶

Back

Close

Full Screen / Esc

Printer-friendly Version

Interactive Discussion



ranging from 0.01 to 5. For surface reflectance, ten modes of surface parameters of the RPV model are used for generating the lookup table (g , $k=-0.1$, 0.2 , g , $k=0.5$, 1.0 , and $\rho_0 = 0.02$ to 0.45 with approximate increments of 0.05). The combination of small and coarse mode, and surface parameters, that yields the best fit to the measurement is used as first guess and a priori in the full retrieval procedure.

4 Aerosol retrieval

4.1 Synthetic retrieval

First, we perform our investigations on a set of 1000 synthetic measurements in the principle plane at solar zenith angle 60.0° . Each synthetic measurement includes 49 equally sampled viewing angles ($\pm 60.0^\circ$ from nadir) and seven of the nine RSP wavelength bands as described in Sect. 2. The relative azimuthal angles are 0.0 and 180.0° for positive and negative viewing zenith angles, respectively. To get subsets with different angular resolution, viewing angles are equally sampled between -60.0 and 60.0° according to the resolution except in subsets with 2 viewing angles for which we use nadir and -60.0° . Aerosol size distribution parameters used here are randomly distributed in their acceptable range for both small mode ($0.1 \leq r_{\text{eff}}^{\text{S}} \leq 0.30 \mu\text{m}$, $0.1 \leq v_{\text{eff}}^{\text{S}} \leq 0.30$) and coarse mode ($0.60 \leq r_{\text{eff}}^{\text{C}} \leq 3.50 \mu\text{m}$, $0.4 \leq v_{\text{eff}}^{\text{C}} \leq 0.6$). To account for the spectral dependence, the refractive indices for each mode are linear combinations of the refractive index spectra as shown in Fig. 2. The aerosol optical thickness τ for each mode varies randomly in the range $0.0 < \tau \leq 0.70$. We consider soil and vegetation land surfaces with parameters $\rho_0 = 0.071(670 \text{ nm})$, $0.159(1590 \text{ nm})$, $0.116(2250 \text{ nm})$, $g = -0.097$, $k = 0.746$ and $\rho_0 = 0.034(670 \text{ nm})$, $0.128(1590 \text{ nm})$, $0.060(2250 \text{ nm})$, $g = -0.071$, $k = 0.725$, respectively (Litvinov et al., 2011). Parameters ρ_0 at all the other RSP wavelengths are obtained by linear interpolation using soil and vegetation surface reflectance provided by ASTER spectral library (Baldrige et al., 2009). For surface reflection of polarized radiance, we use parameters $\alpha = 4.260$, $\sigma = 0.589$

Aerosol retrieval from RSP measurements

L. Wu et al.

Title Page

Abstract

Introduction

Conclusions

References

Tables

Figures



Back

Close

Full Screen / Esc

Printer-friendly Version

Interactive Discussion



and $\alpha = 2.707$, $\sigma = 0.648$ in the modified Fresnel model for soil and vegetation surfaces, respectively (Litvinov et al., 2011). The forward model as described in Sect. 3 was used to simulate the intensity vector at the altitude of RSP (20 km) for all 1000 combinations input parameters. In our simulation, to account for measurement uncertainties, we add a random noise of 2.0% on intensity I and 0.2% on polarization degree P .

4.1.1 Spectral dependent refractive index

We first test the effect of spectral variation of refractive index in the retrieval. The used measurements which are subset of the 1000 synthetic measurements have wavelength range of 410–2250 nm and angular resolution of 13. We consider retrievals to be successfully converged if the χ^2 of the fit ≤ 2.0 , where χ^2 is defined as $\frac{1}{N} \sum_{i=1}^N \left(\frac{y_i - f_i}{s_i}\right)^2$ in which N is the number of measurements, y_i is the measurement, f_i is the simulated result and s_i is the error of the measurement. We found that this χ^2 threshold yields a reasonable balance between accuracy and number of converged cases. Figure 3 compares retrieved refractive indices (at 670 nm) of small and coarse mode with true values for retrievals using a constant and a wavelength-dependent refractive index. The general trend is that, for small mode aerosols, as expected, both approaches yield similar results, while for coarse mode aerosols considering the spectral variation improves the agreement between retrieved and true values for both real and imaginary part of refractive index. Figure 3 shows that before (top panel) and after (bottom panel) including the spectral variation of refractive index in the retrieval, the correlation coefficients for real and imaginary refractive index of coarse mode are 0.78 (top), 0.65 (top), 0.96 (bottom) and 0.35 (bottom), respectively. Most importantly, the number of retrievals that converges with a sufficiently good fit to the measurement ($\chi^2 \leq 2.0$) is more than doubled, from 35.3 to 75.1%.

4.1.2 Comparison between measurement subsets

To investigate the importance of spectral range and angular resolution, we investigate retrieval errors on τ_{550} (AOT), ω_{550} (single scattering albedo, SSA), $r_{\text{eff}}^{\text{S}}$, $v_{\text{eff}}^{\text{S}}$, $r_{\text{eff}}^{\text{C}}$, $v_{\text{eff}}^{\text{C}}$, m_{r}^{S} , m_{i}^{S} , m_{r}^{C} , and m_{i}^{C} using different subsets of the 1000 synthetic measurements. Here we focus on four different wavelength ranges, namely 410–670, 410–865, 410–1590, and 410–2250 nm. The angular resolution changes between 2 and 49. Although the number of cases that converge to $\chi^2 \leq 2.0$ may change per subset, we slightly adjust the χ^2 threshold for each subset so that the convergence percentage is 75% for all subsets.

Figure 4 shows the results of mean absolute errors of each parameter as a function of the number of viewing angles (N) for the four wavelength ranges. The shaded areas indicate the target accuracy on aerosol parameters formulated by Mishchenko et al. (2004) for the APS instrument. First of all, for all four wavelength ranges, the mean errors of parameters are significantly decreased when the number of viewing angles N is increased from 2 to 3. The decrease after $N \geq 3$ is moderate in compared with the change of 2 to 3. The mean errors do not improve anymore when the number N is greater than ~ 10 . Moreover, Fig. 4 also shows the advantage of the 410–1590 and 410–2250 nm subsets, as they yield smaller retrieval errors than subsets with a smaller spectral range. If compared with the 410–670 and 410–865 nm cases, the mean error on the AOT at 550 nm τ_{550} is reduced from ~ 0.1 and ~ 0.06 to ~ 0.04 as shown in the upper left figure. The mean error on the SSA at 550 nm ω_{550} is less than 0.02 while for the 410–670 nm case the errors are around 0.03. The measurements of 410–1590 and 410–2250 nm yield smaller errors especially for the coarse mode. For example, the mean error on the effective radius $r_{\text{eff}}^{\text{C}}$ is reduced from ~ 0.3 to $\sim 0.2 \mu\text{m}$ and the mean error on the real and imaginary refractive index are also reduced. This is attributable to the fact that short-wave infrared bands are sensitive to coarse mode aerosols. For small mode aerosols, the measurements of 410–865 nm performs almost equally well as retrievals including short-wave infrared bands. Finally, the 410–670 nm case usu-

Title Page

Abstract

Introduction

Conclusions

References

Tables

Figures



Back

Close

Full Screen / Esc

Printer-friendly Version

Interactive Discussion



Aerosol retrieval from RSP measurements

L. Wu et al.

Title Page

Abstract

Introduction

Conclusions

References

Tables

Figures



Back

Close

Full Screen / Esc

Printer-friendly Version

Interactive Discussion



ally produces the largest mean error for all parameters. In contrast, the 410–2250 nm case can meet the target accuracy requirements indicated by shaded area for nearly all parameters. If we compare retrievals in the range 410–1590 nm with retrievals in the range 410–2250 nm, we see that the aerosol optical thickness is slightly more accurately retrieved for the latter setup, while for the other parameters the performance is similar.

Figure 5 shows scatterplots of retrieved vs. true values for τ_{550} , ω_{550} and size parameters of both aerosol modes when the viewing angle number $N = 13$ using the full spectral range 410–2250 nm. The comparison between refractive index of both modes is shown in Fig. 3. The correlation coefficients between true and retrieved values for each parameter are 0.98 (τ_{550}), 0.98 (ω_{550}), 0.94 (small mode effective radius $r_{\text{eff}}^{\text{S}}$), 0.73 (small mode effective variance $v_{\text{eff}}^{\text{f}}$), 0.84 (small mode real refractive index m_r^{f}), 0.96 (small mode imaginary refractive index m_i^{f}), 0.92 (coarse mode effective radius $r_{\text{eff}}^{\text{C}}$), 0.44 (coarse mode effective variance $v_{\text{eff}}^{\text{C}}$), 0.96 (coarse mode real refractive index m_r^{C}), and 0.35 (coarse mode imaginary refractive index m_i^{C}). The retrievals of the imaginary part of the coarse model aerosol can be poor when small mode aerosols dominate. However, as shown in Fig. 5, the retrieved single scattering albedo values agree well with true values which indicate good retrievals on total absorption.

4.2 Aerosol retrieval using the RSP data

We applied our algorithm described above to RSP data over land close (distance ≤ 20 km) to AERONET stations so that we can compare our results with independent measurements. The data were pre-processed as described in Sect. 2. Retrievals are made only on cloud-free measurements because clouds are not included in the forward model. Time differences between the RSP measurements and AERONET products are restricted to less than one hour. We use the level 2 direct sun products for AOT comparison and level 1.5 inversion products for refractive index and single scattering albedo comparison with the additional constraint that $\tau_{670} > 0.1$ at 670 nm. In the prod-

Aerosol retrieval from RSP measurements

L. Wu et al.

Title Page

Abstract

Introduction

Conclusions

References

Tables

Figures

◀

▶

◀

▶

Back

Close

Full Screen / Esc

Printer-friendly Version

Interactive Discussion



ucts, aerosol optical thickness values are provided at wavelengths from 340 to 1640 nm with an estimated uncertainty of 0.01–0.02, which are very well suited for validation of the retrieved AOT. Apart from this, they also include micro-physical aerosol properties products, but it is difficult to compare continuous size distribution in AERONET with the small and coarse mode effective radius and effective variance retrieved from RSP. Here we mainly compare AOT and SSA with AERONET. Apart from this, AERONET retrieves one refractive index whereas we retrieve refractive indices for both the small and coarse mode. To get a general impression on the agreement between AERONET and RSP retrieval, we compose a refractive index m_{comp} that is a weighted average by AOT τ of each mode,

$$m_{\text{comp}} = \frac{m^s \tau_s + m^c \tau_c}{\tau_s + \tau_c}. \quad (5)$$

The weighted refractive index m_{comp} should reflect to some extent the retrieval capability on this quantity (Hasekamp et al., 2011).

In our RSP retrieval, we consider cases that passed a goodness of fit criterion under $\chi^2 \leq 10.0$. The threshold here is larger than the one we used in synthetic retrieval, because some measurements are still hampered by angular oscillations caused by inhomogeneity of the underlying surface. Besides, we exclude cases with a minimum scattering angle larger than 85.0° or with a maximum scattering angle less than 155.0° because retrieval errors in those cases are considerably larger than others due to a relatively small range of scattering angle (Hasekamp and Landgraf, 2007). Figure 6 shows one example of RSP measurements and the corresponding fit results for DOLP in retrieval. Generally, the fits are good for each spectral band. In some cases, the measurements can be found to fluctuate between some viewing angles, thus making the fits worse (see the fit for 670 nm in Fig. 6).

Figure 7 shows a comparison between the retrieved AOT from RSP measurements and the AOT provided by AERONET at 440, 675, and 870 nm. Here we show both retrieval results for the 410–1590 and 410–2250 nm cases. From Fig. 7 it follows that

retrieved AOTs at the three wavelengths are in good agreement with the AERONET results. The correlation coefficients are 0.98 for 440 nm, 0.97 for 675 nm and 0.90 for 870 nm.

Figures 8 and 9 show the values of the SSA, refractive index m and the corresponding AERONET values at 675 nm. As stated above, comparison are made only when $\tau_{670} \geq 0.1$. For the SSA, the retrieval results agree reasonably well with AERONET values, especially when using the full spectral range 410–2250 nm. The mean absolute difference in SSA between AERONET and RSP (both cases) is 0.04. Under crude assumption that the AERONET refractive index can be approximated by the weighted average of the two modes, the retrieved values are relatively close to those provided by AERONET.

Figure 10 shows the difference in AOT between RSP and AERONET as a function of the number of viewing angles used in the retrieval. Due to the limited number of cases for which AERONET SSA and refractive index measurements are available, we restrict the analysis to AOT only. We should notice that with the increase of N the retrieval performance sometimes becomes even a bit worse, this is due to the fact that the measurements at some viewing directions can be distorted by the inhomogeneity of the land surface. In general, the results of Fig. 10 confirm our findings from the study with synthetic measurements: (1) the strongest improvement in accuracy is seen when N increases from 2 to 3; (2) the retrieval performances are not further improved if more than 10 viewing angles are used in the retrieval; (3) retrievals perform significantly better when shortwave infrared bands are included.

5 Conclusions

In this paper we performed aerosol retrievals from multi-angle photo-polarimetric measurements produced synthetically and performed by the airborne RSP instrument. We adjusted the SRON aerosol retrieval algorithm to cope with spectral dependent refractive indices so that it can be applied to the full range of RSP.

Aerosol retrieval from RSP measurements

L. Wu et al.

Title Page

Abstract

Introduction

Conclusions

References

Tables

Figures



Back

Close

Full Screen / Esc

Printer-friendly Version

Interactive Discussion



Aerosol retrieval from
RSP measurements

L. Wu et al.

Title Page

Abstract

Introduction

Conclusions

References

Tables

Figures

◀

▶

◀

▶

Back

Close

Full Screen / Esc

Printer-friendly Version

Interactive Discussion



We investigated the capability of different retrieval setups with varying spectral ranges and angular resolutions by considering 1000 synthetic measurements for different aerosol scenarios. We find that the errors on the retrieved parameters were significantly decreased when including multiple viewing geometries. This tendency becomes moderate when $N \geq 3$ and flat after $N \geq 10$. It should be noted however that for future instrumentation a higher number of viewing angles is still desirably in order to separate scattering by aerosols and cloud droplets by means of the rainbow (Waquet et al., 2009b; Hasekamp, 2010) and for the retrieval of cloud microphysical quantities (Alexandrov et al., 2012). Moreover, we demonstrated the advantage of including short-wave infrared bands in the retrieval over retrievals restricted to the visible spectral range. This improvement is in particular significant for coarse mode aerosol parameters such as effective radius and refractive index.

In retrievals from real RSP measurements, the retrieved AOT using short-wave infrared spectral bands agrees well with AERONET products. The correlation coefficients are 0.98 (440 nm), 0.97 (675 nm), and 0.90 (870 nm). The retrieved SSA also agrees well with AERONET although it should be noted that the number of comparison points is limited. The retrieved refractive index averaged over the two modes is consistent with the AERONET refractive index. The results of retrievals for different subsets of RSP measurements with different spectral ranges and angular resolutions confirm the findings of the synthetic study.

Appendix: Models for surface reflection of radiance and polarized radiance

The Rahman Pinty Verstraete model (RPV) is used with the following form:

$$R_l(\lambda, \vartheta_v, \vartheta_0, \phi) = \frac{(\cos \vartheta_0 \cos \vartheta_v)^{k-1}}{(\cos \vartheta_0 + \cos \vartheta_v)^{1-k}} \rho_0(\lambda) F(\gamma) (1 + R(G)). \quad (1)$$

$$F(\gamma) = \frac{1 - g^2}{(1 + g^2 - 2g \cos \gamma)^{1.5}} \quad (2)$$

Aerosol retrieval from RSP measurements

L. Wu et al.

Title Page

Abstract

Introduction

Conclusions

References

Tables

Figures

◀

▶

◀

▶

Back

Close

Full Screen / Esc

Printer-friendly Version

Interactive Discussion



$$1 + R(G) = 1 + \frac{1 - \rho_0}{1 + G} \quad (3)$$

$$G = \sqrt{\tan^2 \vartheta_0 + \tan^2 \vartheta_v - 2 \tan \vartheta_0 \tan |\vartheta_v| \cos \phi} \quad (4)$$

Here ρ_0 , g and k are three independent parameters; λ is wavelength, γ is scattering angle, ϕ is the difference of azimuth angles: $\phi = \phi_v - \phi_0$, ϑ_v and ϑ_0 are viewing and solar zenith angles, respectively; $F(\gamma)$ is Henyey–Greenstein phase function, $1 + R(G)$ is an approximation of the hot spot effect.

The modified Fresnel model is written as,

$$R_p(\vartheta_v, \vartheta_0, \phi) = \frac{\alpha \pi F_p(m, \gamma)}{4(\mathbf{u})_n (\cos \vartheta_v + \cos \vartheta_0)} f((\mathbf{n})_v, (\mathbf{n})_0) f_{\text{sh}}(\gamma). \quad (5)$$

$$f((\mathbf{n})_v, (\mathbf{n})_0) = \frac{1}{\pi \mu_n^3 2 \sigma^2} \exp\left(-\frac{1 - \mu_n^2}{\mu_n^2 2 \sigma^2}\right) \quad (6)$$

$$f_{\text{sh}}(\gamma) = \left(\frac{1 + \cos k_\gamma (\pi - \gamma)}{2}\right)^3 \quad (7)$$

Here $f((\mathbf{n})_v, (\mathbf{n})_0)$ is a Gaussian function which describes the distribution of facets over orientation, where σ is the SD of surface facet slopes. $f_{\text{sh}}(\gamma)$ is a shadowing function with free parameter k_γ . $F_p(m, \gamma)$ is the element F_{21} of the Fresnel scattering matrix with refractive index m . α is a scaling parameter. $(\mathbf{n})_0$ and $(\mathbf{n})_v$ are vectors with form $(\sin \vartheta_0 \cos \phi_0, \sin \vartheta_0 \sin \phi_0, \cos \phi_0)$ and $(\sin |\vartheta_v| \cos \phi_v, \sin |\vartheta_v| \sin \phi_v, \cos \phi_v)$. $(\mathbf{u})_n$ is defined by $\frac{n_v^z + n_0^z}{|(\mathbf{n})_v + (\mathbf{n})_0|}$, where n_v^z and n_0^z are z components of the vector $(\mathbf{n})_v$ and $(\mathbf{n})_0$.

Acknowledgements. The RSP data from the SEAC⁴RS and PODEX field experiments that is used in this study was funded by the NASA Radiation Sciences Program managed by Hal Maring and by the NASA Earth Science Division as part of the pre-formulation study for the Aerosol Cloud and ocean Ecosystem (ACE) mission. L. Wu was supported by a grant from the China Scholarship Council (201306690014).

References

- Alexandrov, M. D., Cairns, B., Emde, C., Ackerman, A. S., and van Diedenhoven, B.: Accuracy assessments of cloud droplet size retrievals from polarized reflectance measurements by the research scanning polarimeter, *Remote Sens. Environ.*, 125, 92–111, 2012. 2808
- 5 Baldridge, A., Hook, S., Grove, C., and Rivera, G.: The aster spectral library version 2.0, *Remote Sens. Environ.*, 113, 711–715, 2009. 2802
- Cairns, B., Russell, E. E., and Travis, L. D.: Research scanning polarimeter: calibration and ground-based measurements, in: SPIE's International Symposium on Optical Science, Engineering, and Instrumentation, International Society for Optics and Photonics, 186–196, 1999. 2795
- 10 D'Almeida, G. A., Koepke, P., and Shettle, E. P.: Atmospheric Aerosols: Global Climatology and Radiative Characteristics, A. Deepak Pub., Hampton, 1991. 2799, 2814
- Dubovik, O., Sinyuk, A., Lapyonok, T., Holben, B. N., Mishchenko, M., Yang, P., Eck, T. F., Volten, H., Munoz, O., Veihelmann, B., Zande, v. d. W. J., Leon, J.-F., Sorokin, M., and Slutsker, I.: Application of spheroid models to account for aerosol particle nonsphericity in remote sensing of desert dust, *J. Geophys. Res.-Atmos.*, 111, D11208, doi:10.1029/2005JD006619, 2006. 2798
- 15 Dubovik, O., Herman, M., Holdak, A., Lapyonok, T., Tanré, D., Deuzé, J., Ducos, F., Sinyuk, A., and Lopatin, A.: Statistically optimized inversion algorithm for enhanced retrieval of aerosol properties from spectral multi-angle polarimetric satellite observations, *Meas. Tech.*, 4, 975–1018, 2011. 2795
- Feng, Y., Ramanathan, V., and Kotamarthi, V. R.: Brown carbon: a significant atmospheric absorber of solar radiation?, *Atmos. Chem. Phys.*, 13, 8607–8621, doi:10.5194/acp-13-8607-2013, 2013. 2799
- 25 Hansen, P. C. and O'Leary, D. P.: The use of the l-curve in the regularization of discrete ill-posed problems, *SIAM J. Sci. Comput.*, 14, 1487–1503, 1993. 2801
- Hasekamp, O. P.: Capability of multi-viewing-angle photo-polarimetric measurements for the simultaneous retrieval of aerosol and cloud properties, *Atmos. Meas. Tech.*, 3, 839–851, doi:10.5194/amt-3-839-2010, 2010. 2795, 2808
- 30 Hasekamp, O. P. and Landgraf, J.: A linearized vector radiative transfer model for atmospheric trace gas retrieval, *J. Quant. Spectrosc. Ra.*, 75, 221–238, 2002. 2798

Aerosol retrieval from RSP measurements

L. Wu et al.

Title Page

Abstract

Introduction

Conclusions

References

Tables

Figures



Back

Close

Full Screen / Esc

Printer-friendly Version

Interactive Discussion



**Aerosol retrieval from
RSP measurements**

L. Wu et al.

Title Page

Abstract

Introduction

Conclusions

References

Tables

Figures



Back

Close

Full Screen / Esc

Printer-friendly Version

Interactive Discussion



Hasekamp, O. P. and Landgraf, J.: Linearization of vector radiative transfer with respect to aerosol properties and its use in satellite remote sensing, *J. Geophys. Res.-Atmos.*, 110, D04203, doi:10.1029/2004JD005260, 2005a. 2798

Hasekamp, O. P. and Landgraf, J.: Retrieval of aerosol properties over the ocean from multispectral single-viewing-angle measurements of intensity and polarization: retrieval approach, information content, and sensitivity study, *J. Geophys. Res.-Atmos.*, 110, D20207, doi:10.1029/2005JD006212, 2005b. 2801

Hasekamp, O. P. and Landgraf, J.: Retrieval of aerosol properties over land surfaces: capabilities of multiple-viewing-angle intensity and polarization measurements, *Appl. Optics*, 46, 3332–3344, 2007. 2794, 2795, 2806

Hasekamp, O. P., Litvinov, P., and Butz, A.: Aerosol properties over the ocean from paraspol multiangle photopolarimetric measurements, *J. Geophys. Res.-Atmos.*, 116, D14204, doi:10.1029/2010JD015469, 2011. 2795, 2801, 2806

Herman, B. M. and Browning, S. R.: A numerical solution to the equation of radiative transfer, *J. Atmos. Sci.*, 22, 559–566, 1965. 2798

IPCC: Climate change 2013: the physical science basis, Intergovernmental Panel on Climate Change, Working Group I Contribution to the IPCC Fifth Assessment Report (AR5), Cambridge Univ. Press, New York, 2013. 2794

Kistler, R., Kalnay, E., Collins, W., Saha, S., White, G., Woollen, J., Chelliah, M., Ebisuzaki, W., Kanamitsu, M., Kousky, V., Dool, v. d. H., Jenne, R., and Fiorino, M.: The ncep-ncar 50-year reanalysis: monthly means cd-rom and documentation, *B. Am. Meteorol. Soc.*, 82, 247–267, 2001. 2797

Knobelspiesse, K., Cairns, B., Mishchenko, M., Chowdhary, J., Tsigaridis, K., van Diedenhoven, B., Martin, W., Ottaviani, M., and Alexandrov, M.: Analysis of fine-mode aerosol retrieval capabilities by different passive remote sensing instrument designs, *Opt. Express*, 20, 21457–21484, 2012. 2795

Landgraf, J., Hasekamp, O. P., Box, M. A., and Trautmann, T.: A linearized radiative transfer model for ozone profile retrieval using the analytical forward-adjoint perturbation theory approach, *J. Geophys. Res.-Atmos.*, 106, 27291–27305, 2001. 2798

Litvinov, P., Hasekamp, O. P., and Cairns, B.: Models for surface reflection of radiance and polarized radiance: comparison with airborne multi-angle photopolarimetric measurements and implications for modeling top-of-atmosphere measurements, *Remote Sens. Environ.*, 115, 781–792, 2011. 2798, 2802, 2803

**Aerosol retrieval from
RSP measurements**

L. Wu et al.

Title Page

Abstract

Introduction

Conclusions

References

Tables

Figures

◀

▶

◀

▶

Back

Close

Full Screen / Esc

Printer-friendly Version

Interactive Discussion



Mishchenko, M. I. and Travis, L. D.: Satellite retrieval of aerosol properties over the ocean using polarization as well as intensity of reflected sunlight, *J. Geophys. Res.-Atmos.*, 102, 16989–17013, 1997. 2794

Mishchenko, M. I., Cairns, B., Hansen, J. E., Travis, L. D. Burg, R., Kaufman, Y. J., Vanderlei Martins, J., and Shettle, E. P.: Monitoring of aerosol forcing of climate from space: analysis of measurement requirements, *J. Quant. Spectrosc. Ra.*, 88, 149–161, 2004. 2804

Nakajima, T. and Tanaka, M.: Algorithms for radiative intensity calculations in moderately thick atmospheres using a truncation approximation, *J. Quant. Spectrosc. Ra.*, 40, 51–69, 1988. 2798

Ottaviani, M., Knobelspiesse, K., Cairns, B., and Mishchenko, M.: Information content of aerosol retrievals in the sunglint region, *Geophys. Res. Lett.*, 40, 631–634, 2013. 2796

Rahman, H., Pinty, B., and Verstraete, M. M.: Coupled surface-atmosphere reflectance (csar) model: 2. semiempirical surface model usable with noaa advanced very high resolution radiometer data, *J. Geophys. Res.-Atmos.*, 98, 20791–20801, 1993. 2798

Schepers, D., aan de Brugh, J., Hahne, P., Butz, A., Hasekamp, O., and Landgraf, J.: Lintran v2.0: A linearised vector radiative transfer model for efficient simulation of satellite-born nadir-viewing reflection measurements of cloudy atmospheres, *J. Quant. Spectrosc. Ra.*, 149, 347–359, 2014. 2798

Smith, L. I.: A Tutorial on Principal Components Analysis, Cornell University, USA, 51, 52, 2002. 2800

Toon, O.: An overview of the studies of emissions and atmospheric composition, clouds and climate coupling by regional surveys (seac4rs) field mission, AGU Fall Meeting Abstracts, Vol. 1, 01, 2013. 2796

Waquet, F., Cairns, B., Knobelspiesse, K., Chowdhary, J., Travis, L. D., Schmid, B., and Mishchenko, M.: Polarimetric remote sensing of aerosols over land, *J. Geophys. Res.-Atmos.*, 114, D01206, doi:10.1029/2008JD010619, 2009a. 2795

Waquet, F., Riedi, J., Labonnote, L., Goloub, P., Cairns, B., Deuzé, J. and Tanré, D.: Aerosol remote sensing over clouds using a-train observations, *J. Atmos. Sci.*, 66, 2468–2480, 2009b. 2808

**Aerosol retrieval from
RSP measurements**

L. Wu et al.

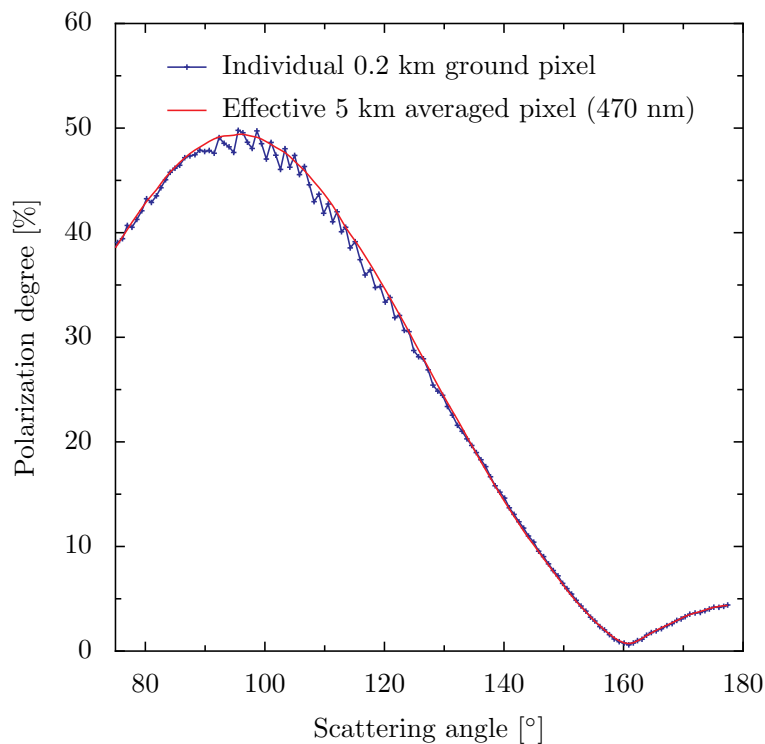


Figure 1. Measurements of individual ground pixel and effective 5 km averaged pixel at 470 nm. Oscillations in angular measurements are due to imperfect co-registration of different viewing angles.

[Title Page](#)[Abstract](#)[Introduction](#)[Conclusions](#)[References](#)[Tables](#)[Figures](#)[◀](#)[▶](#)[◀](#)[▶](#)[Back](#)[Close](#)[Full Screen / Esc](#)[Printer-friendly Version](#)[Interactive Discussion](#)

Aerosol retrieval from
RSP measurements

L. Wu et al.

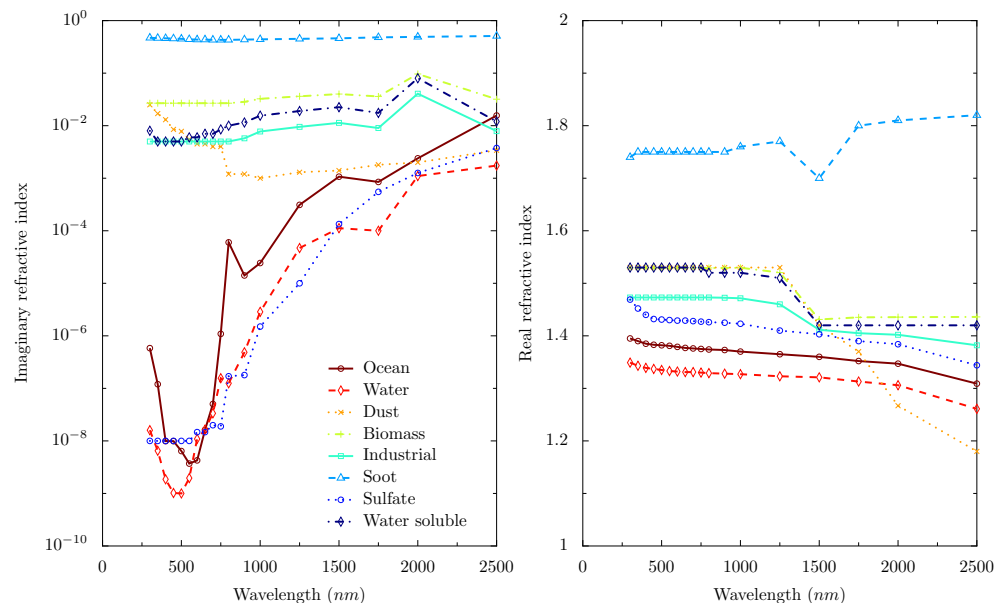


Figure 2. Imaginary (left panel) and real parts (right panel) of the refractive index as a function of wavelength. Data taken from D’Almeida et al. (1991).

[Title Page](#)[Abstract](#)[Introduction](#)[Conclusions](#)[References](#)[Tables](#)[Figures](#)[Back](#)[Close](#)[Full Screen / Esc](#)[Printer-friendly Version](#)[Interactive Discussion](#)

Aerosol retrieval from
RSP measurements

L. Wu et al.

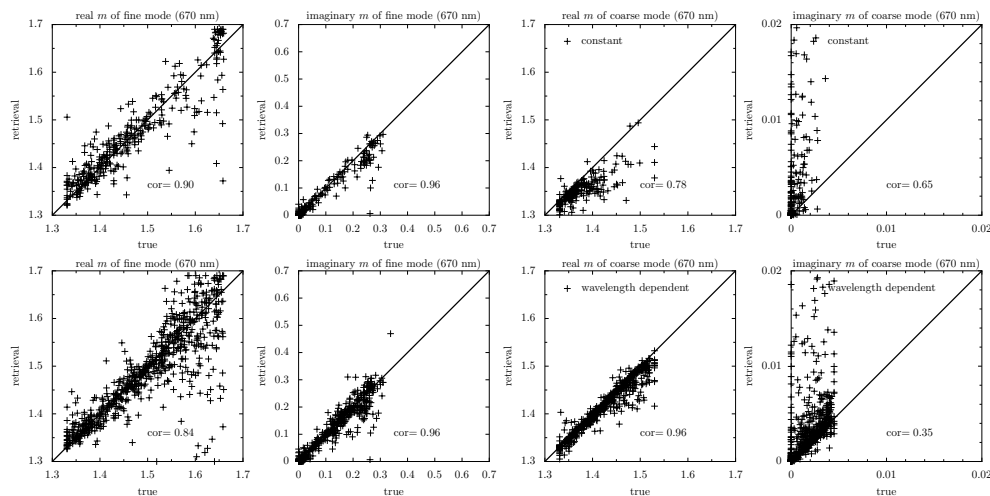


Figure 3. Comparison between before (top panel, for $\chi^2 \leq 2.0$, 35.3% cases converged) and after (bottom panel, 75.1% converged) taking spectral variation of refractive index into account for synthetic retrievals. The correlation coefficients (cor) between retrieved and true values of refractive index are included.

Title Page

Abstract

Introduction

Conclusions

References

Tables

Figures



Back

Close

Full Screen / Esc

Printer-friendly Version

Interactive Discussion



Aerosol retrieval from
RSP measurements

L. Wu et al.

Title Page

Abstract

Introduction

Conclusions

References

Tables

Figures



Back

Close

Full Screen / Esc

Printer-friendly Version

Interactive Discussion

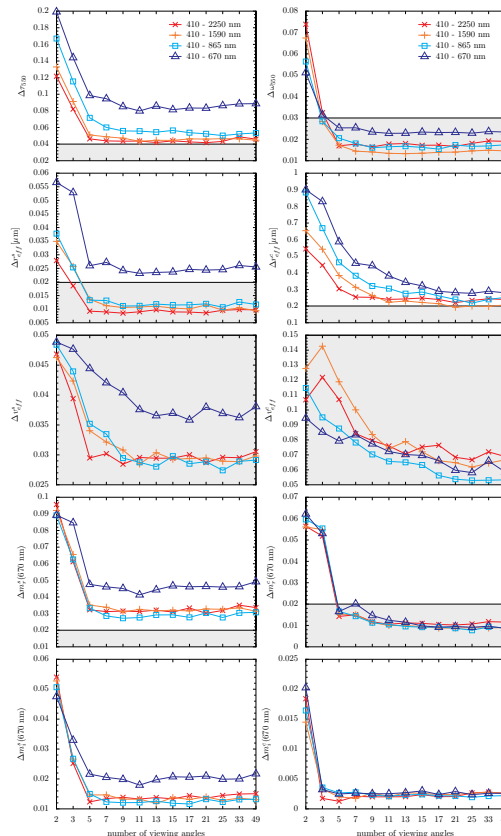


Figure 4. The results of mean absolute errors of aerosol optical thickness (τ_{550}), single scattering albedo (ω_{550}), aerosol size parameters (r_{eff}^s , v_{eff}^s , r_{eff}^c and v_{eff}^c), and refractive index (m_r^s , m_i^s , m_r^c and m_i^c) as a function of the number of viewing angles between retrieved and true values for four different RSP measurement subsets. Soil and vegetation surfaces are used in simulation. Aerosol types in Fig. 2 are all included in simulation and spectral variation of refractive index are included in both simulation and retrieval.

Aerosol retrieval from
RSP measurements

L. Wu et al.

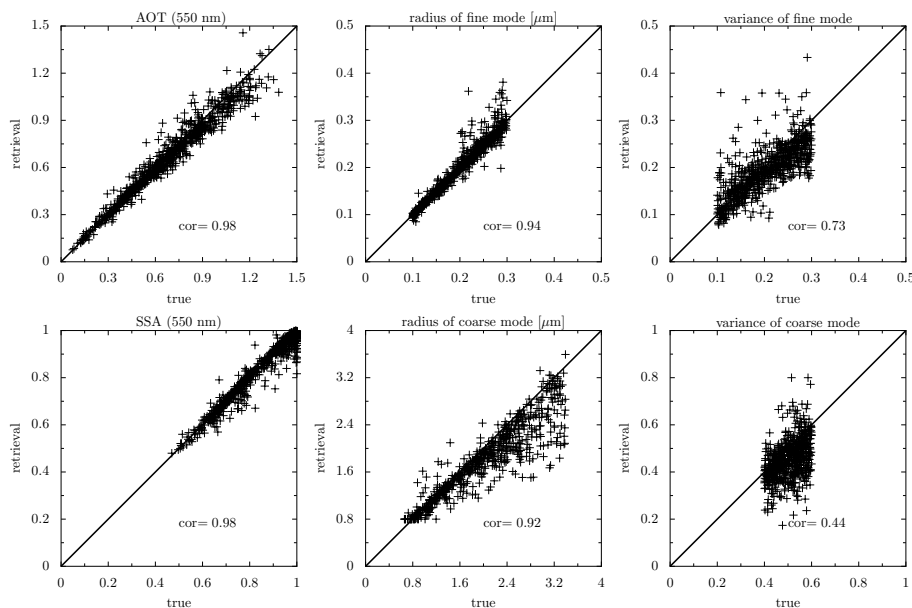


Figure 5. Comparison between retrieved and true values of aerosol optical thickness (τ_{550}), single scattering albedo (ω_{550}), aerosol size parameters ($r_{\text{eff}}^{\text{S}}$, $v_{\text{eff}}^{\text{S}}$, $r_{\text{eff}}^{\text{C}}$ and $v_{\text{eff}}^{\text{C}}$) when the viewing angle number $N = 13$ using the full spectral range 410–2250 nm. The correlation coefficients (cor) are included.

Title Page

Abstract

Introduction

Conclusions

References

Tables

Figures

◀

▶

◀

▶

Back

Close

Full Screen / Esc

Printer-friendly Version

Interactive Discussion



**Aerosol retrieval from
RSP measurements**

L. Wu et al.

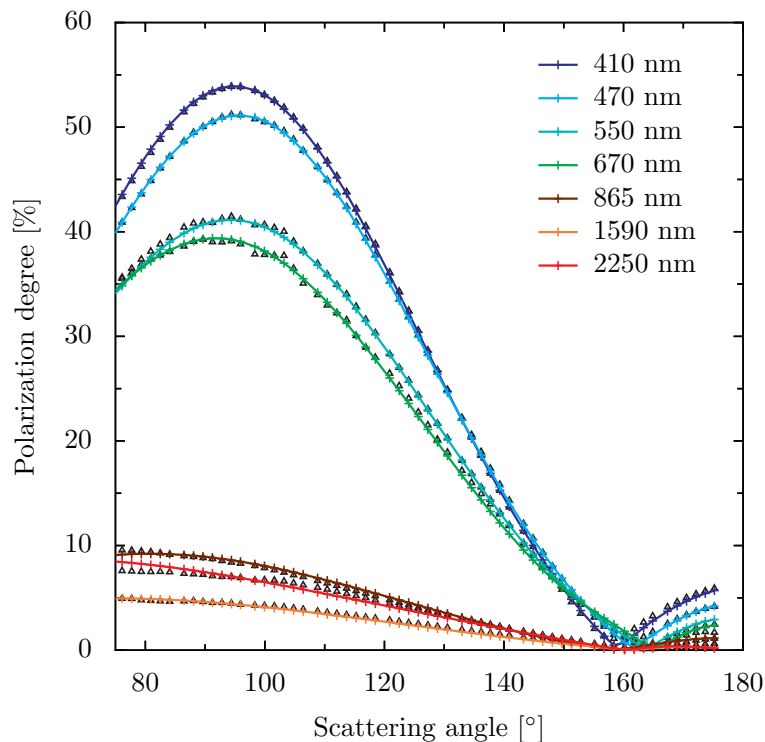


Figure 6. One example of RSP measurements and the corresponding fit results for DOLP in retrieval. Triangle symbols denote the RSP measurements and solid lines with plus are fits using the forward model in Sect. 3. The dates, geolocations (latitude, longitude), and solar zenith angle are 9 September 2013, (-91.7° , 32.3°), and 66.5° .

[Title Page](#)[Abstract](#)[Introduction](#)[Conclusions](#)[References](#)[Tables](#)[Figures](#)[◀](#)[▶](#)[◀](#)[▶](#)[Back](#)[Close](#)[Full Screen / Esc](#)[Printer-friendly Version](#)[Interactive Discussion](#)

Aerosol retrieval from
RSP measurements

L. Wu et al.

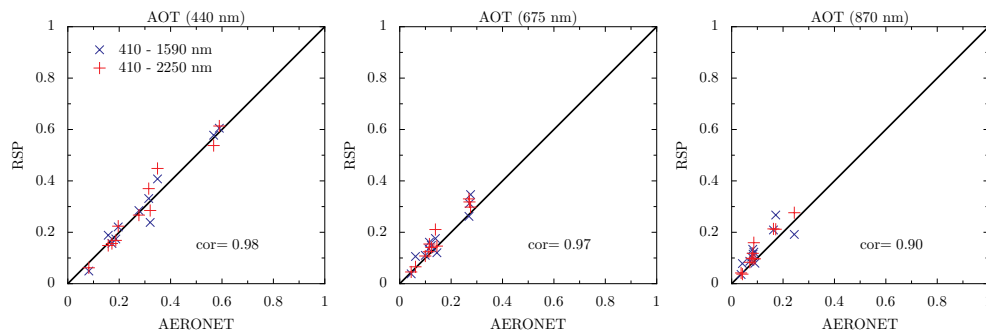


Figure 7. Comparison between the retrieved AOT of RSP measurements and AERONET at 440, 675, and 870 nm. The correlation coefficients (cor) at each wavelength are included.

[Title Page](#)[Abstract](#)[Introduction](#)[Conclusions](#)[References](#)[Tables](#)[Figures](#)[◀](#)[▶](#)[◀](#)[▶](#)[Back](#)[Close](#)[Full Screen / Esc](#)[Printer-friendly Version](#)[Interactive Discussion](#)

Aerosol retrieval from
RSP measurements

L. Wu et al.

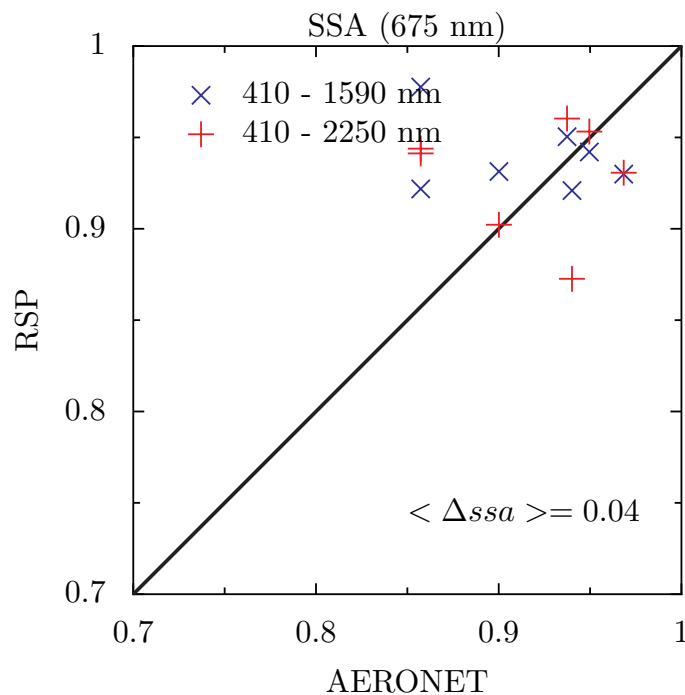


Figure 8. Retrieved single scattering albedo (SSA) of RSP measurements and those provided by AERONET at 675 nm. $\langle \Delta ssa \rangle$ is the mean absolute difference of SSA between RSP and AERONET.

Title Page

Abstract

Introduction

Conclusions

References

Tables

Figures

◀

▶

◀

▶

Back

Close

Full Screen / Esc

Printer-friendly Version

Interactive Discussion



Aerosol retrieval from
RSP measurements

L. Wu et al.

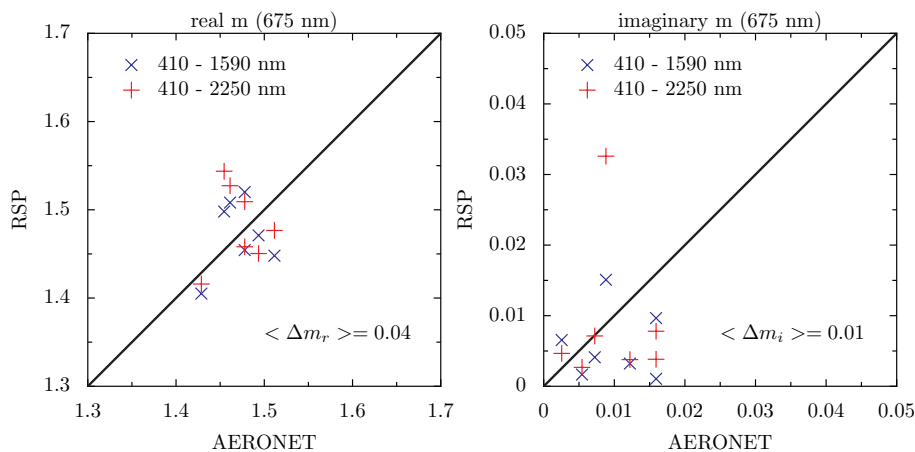


Figure 9. Comparison between composed refractive index of RSP measurements and AERONET at 675 nm. $\langle \Delta m_r \rangle$ and $\langle \Delta m_i \rangle$ are the mean absolute difference of real and imaginary part between RSP and AERONET.

Title Page

Abstract

Introduction

Conclusions

References

Tables

Figures

◀

▶

◀

▶

Back

Close

Full Screen / Esc

Printer-friendly Version

Interactive Discussion



Aerosol retrieval from
RSP measurements

L. Wu et al.

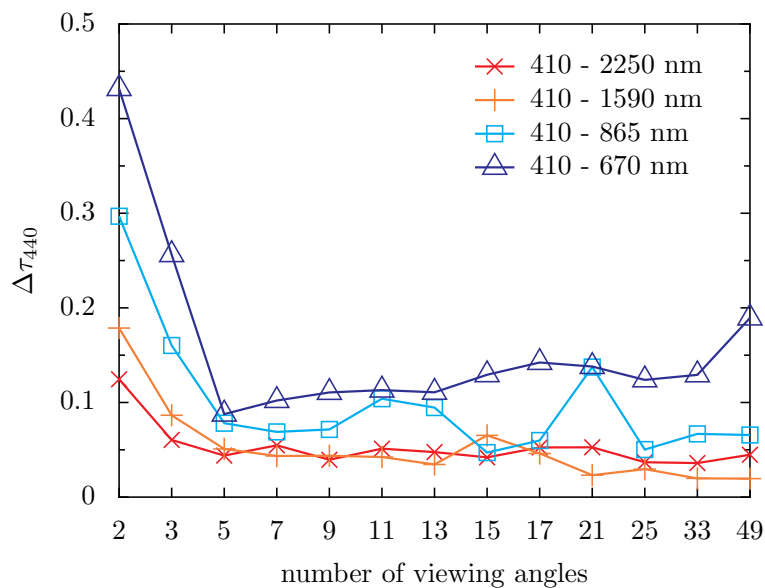


Figure 10. Retrieved AOT mean absolute error dependence on number of viewing angles for different spectral ranges of RSP data.

[Title Page](#)[Abstract](#)[Introduction](#)[Conclusions](#)[References](#)[Tables](#)[Figures](#)[◀](#)[▶](#)[◀](#)[▶](#)[Back](#)[Close](#)[Full Screen / Esc](#)[Printer-friendly Version](#)[Interactive Discussion](#)